CrossMark

Electrical and Mechanical Properties of 3D-Printed Graphene-Reinforced Epoxy

BRETT G. COMPTON,[1,4] NADIM S. HMEIDAT,[1] ROBERT C. PACK,[2] MAXIMILIAN F. HERES,[3] and JOSHUA R. SANGORO[3]

1.—Mechanical, Aerospace, and Biomedical Engineering Department, University of Tennessee, Knoxville, TN, USA. 2.—Materials Science and Engineering Department, University of Tennessee, Knoxville, TN, USA. 3.—Chemical and Biomolecular Engineering Department, University of Tennessee, Knoxville, TN, USA. 4.—e-mail: bcompto1@utk.edu

Recent developments in additive manufacturing have demonstrated the potential for thermoset polymer feedstock materials to achieve high strength, stiffness, and functionality through incorporation of structural and functional filler materials. In this work, graphene was investigated as a potential filler material to provide rheological properties necessary for direct-write three-dimensional (3D) printing and electrostatic discharge properties to the printed component. The rheological properties of epoxy/graphene mixtures were characterized, and printable epoxy/graphene inks formulated. Sheet resistance values for printed epoxy/graphene composites ranged from 0.67×10^2 Ω/sq to 8.2×10^3 Ω/sq. The flexural strength of printed epoxy/graphene composites was comparable to that of cast neat epoxy (~ 80 MPa), suggesting great potential for these new materials in multifunctional 3D-printed devices.

INTRODUCTION

Additive manufacturing (AM) of polymer matrix composites has received growing attention in recent years[1–4] as researchers seek to develop new feedstock materials that address the low stiffness and strength of unreinforced thermoplastic polymers—predominantly acrylonitrile butadiene styrene (ABS) and poly(lactic acid) (PLA)—that are most widely used in material extrusion AM technologies. Printed thermoplastic materials also suffer from weak layer-to-layer bonding[5–9] that can be exacerbated by addition of fibers and other structural filler materials,[6,8,10] and warping due to thermal gradients and stresses that develop during printing.[11–14]

Although rapid improvements are being made in thermoplastic AM, thermoset polymer materials—those that undergo an irreversible crosslinking reaction—have shown significant promise as feedstock materials for direct-write (DW) AM for their high strength, stiffness, chemical resistance, thermal properties, and compatibility with existing structural and functional filler materials.[15–23] Specifically, printed epoxy/carbon fiber composite achieved elastic modulus up to 57 GPa in the print direction using ultrahigh-modulus pitch-based carbon fibers,[22] and strength up to 100 MPa transverse to the print direction, with glass-transition temperatures up to 160°C, using functionalized nanoclay platelets.[19]

Development of thermoset feedstocks for AM is still in its infancy, but these examples indicate the great potential for creating new materials that enable three-dimensional (3D) printing of high-strength multifunctional components and devices. DW feedstocks require strong shear-thinning and pseudoplastic flow behavior that enables deposition through fine nozzles and printing of entire components without requiring immediate curing after deposition. These rheological properties are usually imparted to thermoset resins by high-aspect-ratio, high-surface-area filler materials; a unique feature of thermoset AM feedstocks is that filler materials can serve a double role, imparting both desirable rheological properties for 3D printing and desirable mechanical reinforcement in the printed, cured component. The viscosifiers that have been used most frequently are fumed silica[15,21,23] or functionalized nanoclay platelets.[16,17,19,22] These

viscosifiers, and the epoxy resins they modify, are electrically insulating, yet in many applications some degree of electron transport may be beneficial; For example, electrostatic discharge (ESD) properties may be required for packaging of sensitive electronic components, or electromagnetic shielding properties may be required at certain locations in printed devices.

In this work, we investigated the potential to utilize high-aspect-ratio graphene flakes in place of nanoclay as a multifunctional viscosifier for composite DW feedstocks. We show that high-aspect-ratio graphene imparts shear-thinning and significantly improved electron transport properties to the epoxy resin. However, graphene-only ink formulations are found not to possess sufficiently high shear yield stress to enable 3D printing of objects consisting of more than a few layers ($\sim$ 2–3 mm in height). Addition of small amounts of functionalized nanoclay rectified this printing deficiency and enabled 3D printing of high-resolution, high-aspect-ratio components with strength comparable to that of neat epoxy resin (80 MPa), while maintaining ESD characteristics.

EXPERIMENTAL PROCEDURES

Formulation and Printing

Epon 826 (Momentive Specialty Chemicals, Inc., Columbus, OH) epoxy resin was utilized with 1-ethyl-3-methylimidazolium dicyanamide (BASF Basionics VS 03, Sigma-Aldrich, Inc., St. Louis, MO) as latent curing agent at ratio of 5 parts per hundred resin, following Ref. 17. Four grades of graphene, viz. N006-P, N008-P-40, N008-P-10, and N008-N (Angstron Materials, Inc., Dayton, OH), having different average aspect ratios were evaluated for their effect on the rheological properties of the epoxy resin and potential for use as a DW ink constituent. Garamite 7305 nanoclay platelets (BYK-Chemie GmbH, Inc., Wesel, Germany) were used to further modify the rheology of the epoxy resin and enhance printing behavior.

Epoxy/graphene ink formulations were prepared using a planetary SpeedMixer (FlackTek, Inc., Landrum, SC). All formulations contained 20 g resin and 1 g VS 03, mixed under vacuum at 0.1 atm for 60 s at 1800 rpm. Graphene was then added, and the formulation was mixed under vacuum at 0.1 atm for 240 s at 1800 rpm. Ink formulations containing nanoclay platelets were mixed for 120 s after adding the graphene, followed by mixing for another 120 s after adding the nanoclay.

The final ink formulations were loaded into 10-cc syringe barrels (Nordson EFD, Westlake, OH) and centrifuged at 3990 rpm for 5 min using a Sorvall^{TM} ST-8 centrifuge (ThermoFisher Scientific, Waltham, MA) to remove bubbles that may have been introduced during the loading process. The loaded syringe barrels were then mounted in a pressure adapter (HP3, Nordson EFD) and mounted on a

three-axis positioning stage (Shopbot Tools, Inc., Durham, NC) for printing. The inks were 3D-printed onto polytetrafluoroethylene (PTFE)-coated aluminum foil substrates (Bytac, Saint-Gobain Performance Plastics, Worcester, MA) using either 335-micron-diameter or 864-micron-diameter tapered metallic luer-lock nozzle tips (S-type, GPD Global, Grand Junction, CO). Print paths were generated in G-code using custom-written scripts in Scilab software (Scilab Enterprises, France). Formulations containing less than 20 wt.% graphene were cast into printed silicone molds. All specimens were cured at 100°C for 24 h followed by 2 h at 220°C.

Characterization

Rheological properties of the inks were measured under ambient conditions using a Discovery Hybrid Rheometer HR-2 (TA Instruments, New Castle, DE). Oscillatory stress sweeps were performed from 5 Pa to 5000 Pa, and flow sweeps were performed from 0.02 to 100 1/s. All measurements were taken using parallel plates with gap size of 0.5 mm. Measurements were preceded by a constant-shear conditioning step of 0.1 1/s for 120 s. Flexural tests were performed at room temperature on an electromechanical load frame (model 45, MTS Systems Corporation, Eden Prairie, MN). Specimens with nominal dimensions of 65 mm × 12.7 mm × 3.2 mm were tested in a three-point flexure using a span of 50 mm and cross-head speed of 1.3 mm/min. The sheet resistance was measured using a Gamry Reference 600 potentiostat/galvanostat (Gamry Instruments, Warminster, PA) in four-electrode configuration over the frequency range from 1 Hz to 10 kHz under ambient conditions with 2-cm-long platinum wire electrodes, separated by 1 cm. The thickness of each sample was determined using a tabletop micrometer. Samples were cleaned using acetone prior to taking measurements, and three measurements were made per sample.

RESULTS AND DISCUSSION

To evaluate the potential of different grades of graphene as viscosifiers in epoxy-based DW inks, a series of rheological measurements were carried out on mixtures comprising epoxy resin and 10 wt.% of four different grades of graphene having different average aspect ratio. The plot of apparent viscosity versus shear rate for each mixture is shown in Fig. 1a. The apparent viscosity of the neat resin was nearly rate independent, indicating predominantly Newtonian behavior. Addition of graphene resulted in an increase in apparent viscosity across all shear rates probed. The apparent viscosity at low shear rate and the degree of shear thinning correlated strongly with the average aspect ratio of the graphene filler, as indicated in the figure. However, the strongest effect on rheology corresponded to
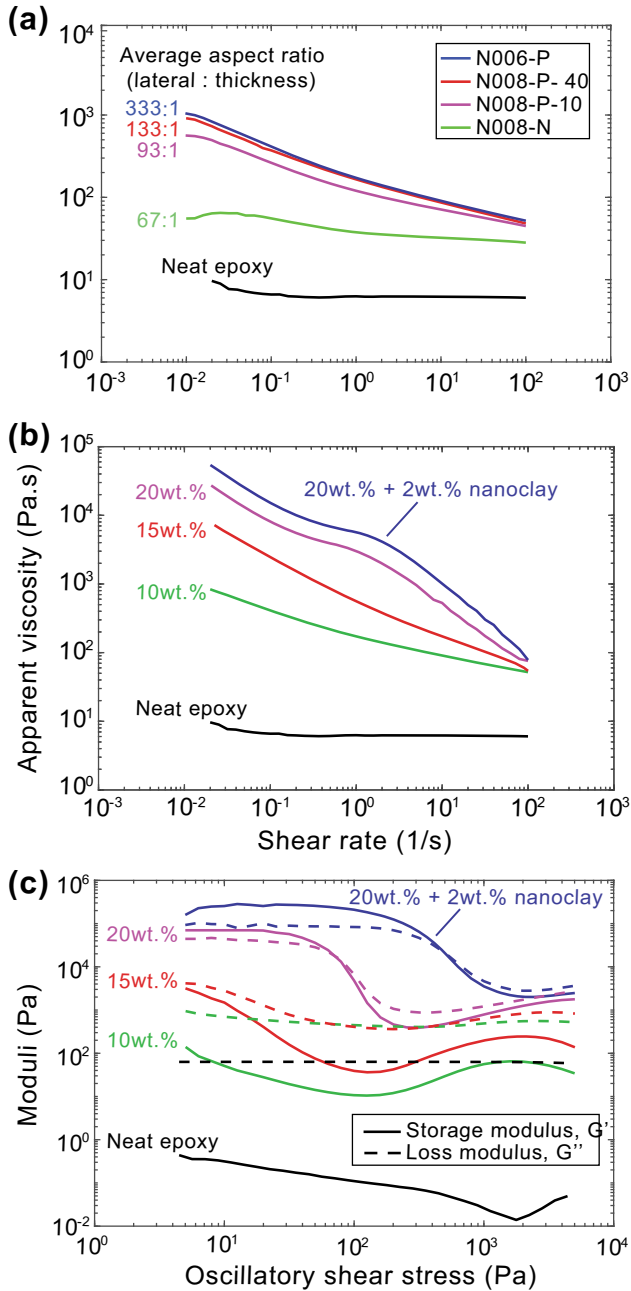
(a)

(b)

(c)

Fig. 1. (a) Apparent viscosity of 10 wt.% graphene formulations containing different grades of graphene. (b) Apparent viscosity of epoxy/graphene formulations containing various amounts of N006-P graphene. (c) Storage and loss moduli for the formulations tested in (b).

Using N006-P graphene, new formulations containing 10 wt.%, 15 wt.%, and 20 wt.% graphene were characterized. Plots of the apparent viscosity versus shear rate are shown in Fig. 1b. The apparent viscosity at 2×10^{-2} 1/s increased from 8×10^2 Pa s for 10 wt.% graphene to 8×10^3 Pa s for 15 wt.% graphene and 2×10^4 Pa s for 20 wt.% graphene. Shear thinning also increased with increasing graphene content, so that the apparent viscosity at shear rates representative of those experienced by ink during deposition ($\sim$ 50 1/s) only increased from 60 Pa s for 10 wt.% graphene to 100 Pa s for 20 wt.% graphene. Addition of 2 wt.% functionalized nanoclay to the formulation with 20 wt.% graphene (referred to hereinafter as the 20 wt.% + clay formulation) increased the apparent viscosity at all shear rates, but did not affect the shear-thinning behavior. This high degree of shear thinning enables viscous inks to be deposited through fine nozzles without requiring excessive driving pressure. The storage and loss moduli for these formulations are shown in Fig. 1c. These measurements provide insight into the solid-like nature of the ink and reflect the ability of the ink to hold its shape after deposition. For both 10 wt.% and 15 wt.% graphene, the loss modulus was higher than the storage modulus throughout the range of stresses probed, indicating that these formulations exhibited liquid-like behavior. However, the 20 wt.% formulation exhibited a shear yield stress—approximated in this case by the value of the oscillatory shear stress at the crossover point for the storage and loss moduli[24]—of 70 Pa, below which the storage modulus was higher than the loss modulus. At stresses below the yield stress, this formulation exhibited the solid-like behavior that is necessary for successful DW inks. Addition of 2 wt.% functionalized nanoclay to the 20 wt.% graphene formulation significantly increased the yield stress to 500 Pa and increased the storage and loss moduli below the yield stress to 2×10^5 Pa and 1×10^5 Pa, respectively.

The surfaces of samples printed using the 20 wt.% and 20 wt.% + clay formulations are shown in Fig. 2a and b, respectively. Printed layers are oriented horizontally in the micrographs, with the build direction oriented vertically. The round or oval surface features correspond to individual printed filaments. The smooth surface of the bottom half of Fig. 2a is a consequence of the low yield stress of the ink. As additional layers are printed, the lower layers are put under stress by the force of the ink exiting the print nozzle, and the lower layers have yielded and flowed together. Conversely, the 20 wt.% + clay formulation possessed sufficiently high yield stress that additional layers did not cause yielding. These results suggest that addition of nanoclay is unnecessary to print low-aspect-ratio structures comprising only a few layers, but is necessary for high-aspect-ratio 3D structures. Using the latter ink, a prototype 50 mm × 50 mm wafer

whether the graphene was polar or nonpolar, indicated by "P" or "N," respectively, in the name of the graphene grade. Because the epoxy resin was polar, stronger interaction would be expected with polar filler materials, and this was indeed observed to be the case. Based on these observations, N006-P graphene, which had the highest aspect ratio and greatest effect on the rheology of the epoxy resin, was selected for use in formulating epoxy/graphene composite inks for DW 3D printing.
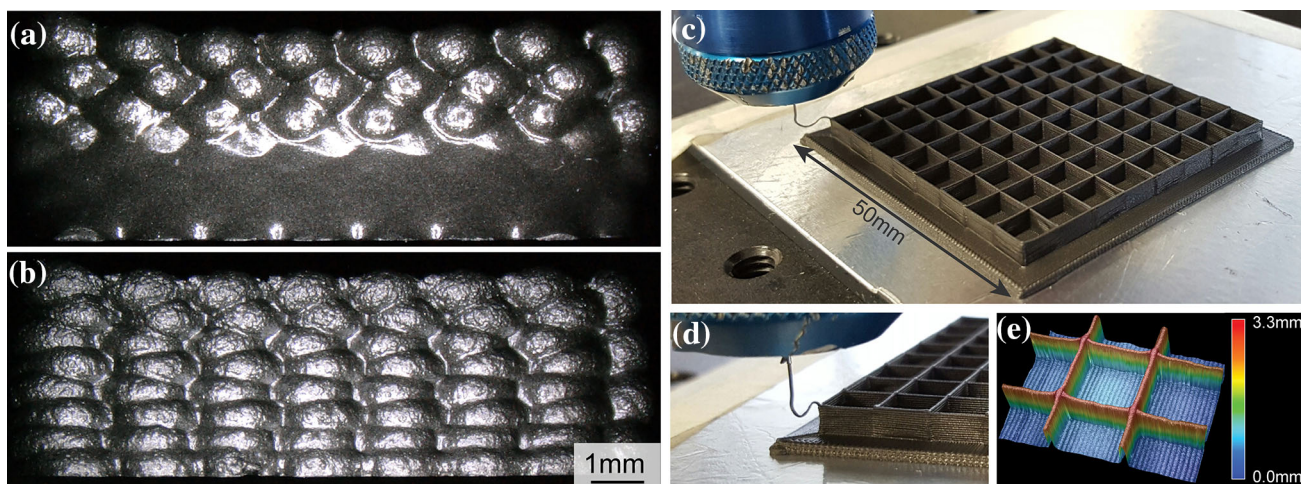
Fig. 2. (a) Optical micrograph of surface of sample printed using the 20 wt.% formulation. (b) Optical micrograph of surface of sample printed using the 20 wt.% + clay formulation. (c, d) Printing of a 50 mm × 50 mm prototype wafer tray using the 20 wt.% + clay formulation. (e) Height map of partitions in the wafer tray, showing high aspect ratio and minimal height variations. The square cells are 5.5 mm on a side.
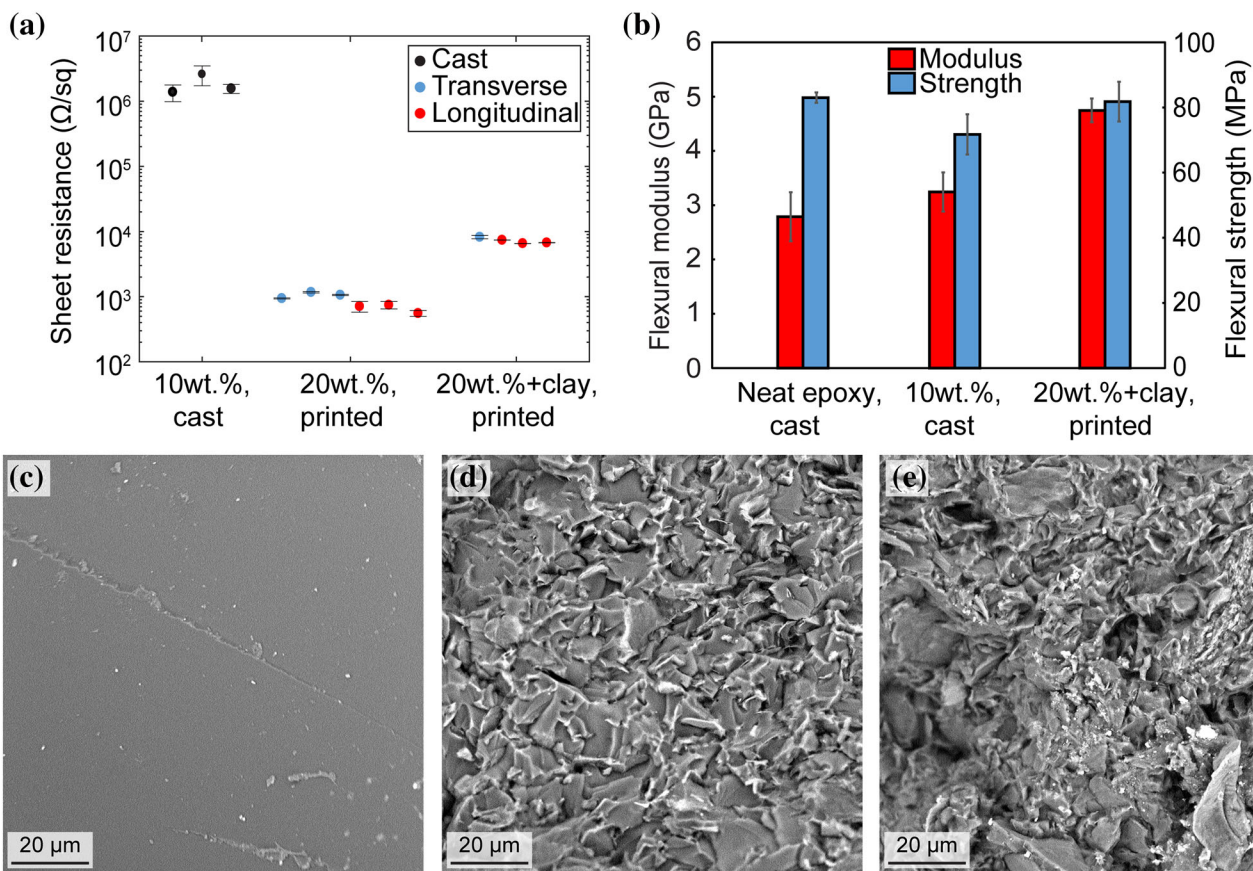

Fig. 3. (a) Electrical properties of printed and cast samples. (b) Flexural modulus and strength of printed and cast samples. (c–e) Scanning electron micrographs of fracture surface of flexural specimens. (c) Cast neat epoxy. (d) Cast epoxy 10 wt.% graphene. (e) Printed epoxy 20 wt.% graphene + clay.

tray was printed to demonstrate the printing behavior and fine resolution achievable with these inks (Fig. 2c and d). The height map of the printed walls in Fig. 2e reveals thin, consistent wall thickness with only minimal variation in the height of the top surface that may indicate slight mismatch between the ink flow rate and print head translation rate.

Sheet resistance values measured for cast 10 wt.% samples, as well as thick films (~ 1 mm thick) printed using the 20 wt.% and 20 wt.% + clay formulations, are shown in Fig. 3a. The average sheet resistance value for the cast 10 wt.% samples was 1.85×10^6 Ω/sq, corresponding to bulk resistivity of 1×10^3 Ω m, approximately five orders of magnitude lower than the resistivity of the neat epoxy resin, reported to be 5×10^8 Ω m.[25] Although the 20 wt.% formulation did not possess sufficient yield stress to print high-aspect-ratio components, thin films were printed for electrical characterization parallel and transverse to the print direction. The average sheet resistance of these samples was measured to be 6.7×10^2 Ω/sq and 1.06×10^3 Ω/sq along and transverse to the print direction, respectively. These values correspond to bulk resistivity values of 0.61 Ω m and 1.08 Ω m, respectively. Meanwhile, 20 wt.% + clay samples were measured to have sheet resistance values of 6.9×10^3 Ω/sq and 8.2×10^3 Ω/sq along and transverse to the print direction, respectively, corresponding to bulk resistivity values of 2.8 Ω m and 2.9 Ω m. From these measurements, it is apparent that the printing process had a small but measureable effect on the directionality of the conductive network within the material due to alignment of the graphene flakes as a result of shear within the deposition nozzle. Presence of nanoclay platelets increased the resistivity of the material by disrupting the graphene network, but the sheet resistance values for this ink are still well below those of other filled polymer materials used for ESD applications.

The flexural properties of the composites are reported in Fig. 3b, and scanning electron micrographs of representative fracture surfaces for each sample are shown in Fig. 3c, d, and e for neat cast epoxy, cast 10 wt.%, and printed 20 wt.% + clay, respectively. Cast neat epoxy displayed flexural modulus of 2.8 GPa and flexural strength of 83 MPa. Cast 10 wt.% samples displayed flexural modulus of 3.2 GPa and strength of 72 MPa. The printed 20 wt.% + clay formulation displayed flexural modulus of 4.7 GPa and strength of 82 MPa along the print direction. The fracture surface of neat epoxy was smooth and glassy, characteristic of brittle failure in unreinforced epoxy, while the fracture surface of the two samples containing graphene was rough and tortuous. No major agglomerates were apparent, indicating that the graphene and clay were well dispersed in the resin. Small flat cleavage patches were visible between graphene flakes in the cast 10 wt.% sample (Fig. 3-d). Crack deflection and pullout of graphene flakes were visible in both samples containing graphene, suggesting that these composites likely possessed higher fracture toughness than neat epoxy alone. The fracture surface of the printed sample (Fig. 3e) did not present the stark evidence of directionality that may be expected from the printing process, but quantitative characterization of the directionality in

these and similar printed nanocomposites is the subject of ongoing research and beyond the scope of the present effort.

CONCLUSION

We evaluated the effects of four different grades of graphene flake on the rheological properties of an epoxy resin, and used one grade to formulate and characterize epoxy/graphene feedstocks for direct-write additive manufacturing. The results show that graphene alone is sufficient as a viscosity modifier to create feedstocks for printing of low-aspect-ratio components with low resistivity. Graphene alone is not sufficient to create feedstocks that can be used to print high-aspect-ratio features, but addition of a small amount of nanoclay to the formulation increased the shear yield stress of the ink without significantly increasing the resistivity of the printed components and enabled printing of high-aspect ratio features with high resolution. Printed epoxy/graphene composites were as strong as cast neat epoxy and 67% stiffer, and possessed low bulk resistivity, making them promising materials for use in ESD applications and multifunctional 3D-printed devices.

ACKNOWLEDGEMENTS

REFERENCES

1. R.D. Farahani, M. Dubé, and D. Therriault, *Adv. Mater.* 28, 28 (2016).
2. T. Hofstätter, D.B. Pedersen, G. Tosello, and H.N. Hansen, *J. Reinf. Plast. Compos.* 36, 15 (2017).
3. P. Parandoush and D. Lin, *Compos. Struct.* 182, 36 (2017).
4. X. Wang, M. Jiang, Z. Zhou, J. Gou, and D. Hui, *Compos. Part B Eng.* 110, 442 (2017).
5. S.H. Ahn, M. Montero, D. Odell, S. Roundy, and P.K. Wright, *Rapid Prototyp. J.* 8, 4 (2002).
6. C.E. Duty, V. Kunc, B. Compton, B. Post, D. Erdman, R. Smith, R. Lind, P. Lloyd, and L. Love, *Rapid Prototyp. J.* 23, 1 (2017).
7. O. Es-Said, J. Foyos, R. Noorani, M. Mendelson, R. Marloth, and B. Pregger, *Mater. Manuf. Process.* 15, 1 (2000).
8. V. Kishore, C. Ajinjeru, A. Nycz, B. Post, J. Lindahl, V. Kunc, and C. Duty, *Addit. Manuf.* 14, 7 (2017).
9. Q. Sun, G. Rizvi, C. Bellehumeur, and P. Gu, *Rapid Prototyp. J.* 14, 2 (2008).
10. M. Shofner, K. Lozano, F. Rodríguez-Macías, and E. Barrera, *J. Appl. Polym. Sci.* 89, 11 (2003).
11. B.G. Compton, B.K. Post, C.E. Duty, L. Love, and V. Kunc, *Addit. Manuf.* 17, 77 (2017).
12. L.J. Love, V. Kunc, O. Rios, C.E. Duty, A.M. Elliott, B.K. Post, R.J. Smith, and C.A. Blue, *J. Mater. Res.* 29, 17 (2014).
13. M. Talagani, S. DorMohammadi, R. Dutton, C. Godines, H. Baid, F. Abdi, V. Kunc, B. Compton, S. Simunovic, and C. Duty, *SAMPE J.* 51, 4 (2015).
14. T.-M. Wang, J.-T. Xi, and Y. Jin, *Int. J. Adv. Manuf. Technol.* 33, 11 (2007).

15. P. Calvert, T.L. Lin, and H. Martin, *High Perform. Polym.* 9, 4 (1997).
16. B.G. Compton, J.W. Kemp, T.V. Novikov, R.C. Pack, C.I. Nlebedim, C.E. Duty, O. Rios, and M.P. Paranthaman, *Mater. Manuf. Process.* (2016). https://doi.org/10.1080/10426914.2016.1221097.
17. B.G. Compton and J.A. Lewis, *Adv. Mater.* 26, 34 (2014).
18. R.D. Farahani, H. Dalir, V. Le Borgne, L.A. Gautier, M.A. El Khakani, M. Levesque, and D. Therriault, *Nanotechnology* 23, 8 (2012).
19. N.S. Hmeidat, J.W. Kemp, and B.G. Compton, *Compos. Sci. Technol.* (2017, in Review).
20. M. Invernizzi, G. Natale, M. Levi, S. Turri, and G. Griffini, *Materials* 9, 7 (2016).
21. J.P. Lewicki, J.N. Rodriguez, C. Zhu, M.A. Worsley, A.S. Wu, Y. Kanarska, J.D. Horn, E.B. Duoss, J.M. Ortega, and W. Elmer, *Sci. Rep.* 7, 43401 (2017).
22. S. Malek, J.R. Raney, J.A. Lewis, and L.J. Gibson, *Bioinspir. Biomim.* 12, 2 (2017).
23. J. Peng, T.L. Lin, and P. Calvert, *Compos. Part A Appl. Sci. Manuf.* 30, 2 (1999).
24. M. Dinkgreve, J. Paredes, M.M. Denn, and D. Bonn, *J. Non-Newton. Fluid Mech.* 238, 33 (2016).
25. S.G. Miller, J.L. Bauer, M.J. Maryanski, P.J. Heimann, J.P. Barlow, J.-M. Gosau, and R.E. Allred, *Compos. Sci. Technol.* 70, 7 (2010).